INTERNATIONAL JOURNAL FOR NUMERICAL METHODS IN FLUIDS, VOL. 8, 199–225 (1988)

A NEW FLUID–STRUCTURE INTERACTION ANALYSIS BASED ON HIGHER-ORDER BOUNDARY ELEMENTS

GRANT E. HEARN AND EDILIO DONATI

Department of Naval Architecture and Shipbuilding, Armstrong Building, The University, Newcastle upon Tyne NE1 7RU, U.K.

SUMMARY

In strip theory analysis the vessel is represented by a series of 2D transverse sections. For 2D arbitrary-shaped sections either floating in the free surface or totally submerged, a higher-order boundary element analysis has been developed to permit determination of the associated radiation and diffraction velocity potentials.

In this paper the formulation of the cited interaction problems is reworked to reflect the new capability of permitting curved boundary elements to represent the geometry and a higher-order functional behaviour of the unknown velocity potentials over that geometry. This is in direct contrast to the usual technique of using straight-line geometric panels and invariant behaviour of the required potentials over these simple panels.

Applications to representative sections of floating ships and the fully submerged pontoon section of a semi-submersible are presented. Within these applications the results of the standard Frank close-fit technique, of linear panels and constant behaviour, are compared with different combinations of higher-order representations of the geometry and the determined velocity potentials.

Conclusions regarding the advantages and limitations of the procedures developed are discussed.

KEY WORDS Strip Theory Boundary Elements Fluid-structure Interactions Radiation Diffraction

INTRODUCTION

The hydrodynamic problems formulated in the determination of the motions and loads on bodies at sea are often simplified by reducing them to a series of two-dimensional boundary value problems. Two-dimensional problems have also received attention in their own right without reference to global problems. Of the methods available for their solution, that involving the use of Green's second identity and a fundamental fluid singularity appropriate to the interaction problem is often used. This approach lies within the broad group of techniques known as boundary element methods (BEM) which are finding increasing application in various engineering disciplines.

In general the method ultimately involves the solution of an integral equation of the second kind. Because of its complexity, numerical methods have to be used except for simple geometries. Hess and Smith[1] pioneered a three-dimensional numerical solution procedure of immense practical application, whereas Frank[2] implemented the corresponding procedure for the case of two-dimensional water wave problems treated in this paper. Without going into too many details, the so-called Frank close-fit procedure consisted of approximating the two-dimensional cross section by means of a series of straight lines and assuming that the unknown function is constant over each of the straight lines. This paper outlines the formulation and implementation of an

0271–2091/88/020199–27$13.50
© 1988 by John Wiley & Sons, Ltd.
Received 21 November 1986

improved procedure whereby it is possible to have curved segments approximating the cross-section and higher-order representations of the unknown function over the segments. The general stimulus for pursuing the study of this advanced method is the achievement of either an increased accuracy for a given number of elements or a reduction in the computational effort required for a given accuracy. All these benefits are of course to be measured relative to the standard implementation of the method.

Having outlined the basic problem, the remainder of the paper is concerned with the development, implementation and application of the higher-order boundary element procedure.

2. FLUID–STRUCTURE INTERACTION FORMULATION

The motion of a vessel oscillating as a result of excitation by an incident wave system can be adequately modelled, within the limitations of a linearized analysis, through solution of the so-called radiation and diffraction problems. In the former set of problems one determines the wave systems and hence the resultant forces or moments acting on the vessel due to the harmonic motion of the structure in otherwise still water. The diffraction problem is concerned with the disturbance of the incident wave field due to the presence of the vessel considered fixed. In each class of problem we are determining the response to a harmonic disturbance and we therefore assume the unknown velocity potential $\Phi(x, y, z, t)$ can be expressed as

$$\Phi(x, y, z, t) = \phi(x, y, z)\exp(-\mathrm{i}\omega t),$$

where ω is the oscillation frequency. Assuming z is the positive forward direction along the longitudinal axis of the vessel, then the strip theory requires solutions of the unknown sets of velocity potentials

$$\{\phi^r(x, y)|z_i\text{fixed}\} \quad \text{and} \quad \{\phi_{D_\theta}(x, y)|z_i\text{fixed}\},$$

where the fixed value of z_i corresponds to the position of the ith transverse section of interest and the superscript r and subscript D_θ denote the rth degree of freedom in the radiation problem and the wave direction θ in the diffraction problem respectively. For beam waves only ($\theta = \pi/2, 3\pi/2$), the diffraction problem, like the radiation problem, is governed by the two-dimensional form of Laplace's equation. For non-beam sea headings, the diffraction potential is assumed to have the same z dependence as the incident wave potential. This assumption reduces the 3D Laplace equation to Helmholtz's equation as the governing equation for the diffraction problem. Clearly this ignores longitudinal interactions of the incident wave with the different transverse sections of the vessel and does not recognize the well known singularity problems associated with strip-theory-orientated diffraction analysis.[3] Here our aim is to simply investigate a new procedure of analysing the classical radiation and diffraction problems associated with strip theory formulations. In either case the Fredholm integral equation to solve can be determined using Green's second identity, namely,

$$\int_S (\psi \nabla^2 \phi - \phi \nabla^2 \psi)\,\mathrm{d}S = \int_C \left(\psi \frac{\partial \phi}{\partial n} - \phi \frac{\partial \psi}{\partial n}\right)\mathrm{d}l$$

and the governing equations
$\nabla^2\Phi = 0$ everywhere in the fluid,
$(\partial\Phi^2/\partial t^2) + g(\partial\Phi/\partial y) = 0$ on the free surface, $y = 0$,
$(\partial\Phi/\partial n) = v_n \exp(-\mathrm{i}\omega t)$ on the wetted surface,
$(\partial\Phi/\partial n) = 0$ on the seabed,

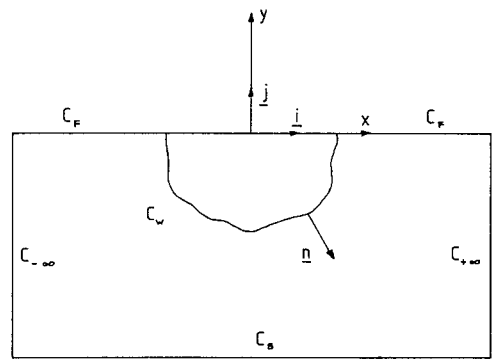

Figure 1. Co-ordinates and domain definition

together with the Sommerfeld radiation condition

$$\lim_{x \to \pm\infty} (\partial/\partial x \mp \mathrm{i}\nu)(\Phi^r, \Phi_{D_\theta}) = 0,$$

where $\nu = \omega^2/g$. Noting the time-harmonic behaviour of the fluid and application of the conditions on each part of the enclosing surface S presented in Figure 1 and made up of the free surface C_F, the vessel's wetted surface C_w, the sea bed C_B and two vertical control lines $C_{\pm\infty}$ some distance from the vessel leads to the well-known integral equation

$$\alpha\phi(p) + \int_{C_w} \left(\phi(q) \frac{\partial G(p,q)}{\partial n_q} - G(p,q) v_n(q) \right) \mathrm{d}l(q) = 0. \tag{1}$$

That is, we shall mainly be concerned with the direct solution of the integral equation for the velocity potential itself. This is in contrast to the indirect BEM approach where the unknown is an auxiliary fictitious function invariably referred to as the source strength.

In equation (1) p and q both define points on C_w with the difference that p is a fixed point and q is the variable of integration. The angle α is equal to π when p is located on a smooth portion of C_w. At a point of discontinuity on C_w, α is the angle measured in radians, from the fluid side, between the two tangent vectors to C_w at p. The angle α arises because on substituting $\psi = G$ in Green's identity, the velocity potential $G(p,q)$ describing the flow due to a pulsating fluid singularity, initially violates the assumptions of the identity. Thus $G(p,q)$, the so-called Green function, represents the velocity potential evaluated at p of a fluid singularity situated at q. For the 2D radiation and diffraction problems governed by Laplace's equation, we have

$$G(p,q) = \ln r - \ln r' + 2PV \int_0^\infty \frac{\mathrm{e}^{k(y+\eta)} \cos[k(x-\xi)]}{\nu - k} \mathrm{d}k$$

$$- 2\pi \mathrm{i} \mathrm{e}^{\nu(y+\eta)} \cos[\nu(x-\xi)]. \tag{2a}$$

For non-beam sea wave diffraction analysis the Green function assumes the form

$$G(p,q) = K_0[Kr] - K_0[Kr'] + 2\nu \int_0^\infty \frac{\mathrm{e}^{-\nu\alpha} K_1[KR](\alpha + y + \eta)}{R} \mathrm{d}\alpha$$

$$-\frac{2\pi\nu}{\sqrt{(\nu^2-K^2)}}e^{\nu(y+\eta)}\sin[|x-\xi|\sqrt{(\nu^2-K^2)}] \tag{2b}$$

$$-\frac{i2\pi\nu}{\sqrt{(\nu^2-K^2)}}e^{\nu(y+\eta)}\cos[|x-\xi|\sqrt{(\nu^2-K^2)}].$$

In the above definitions the following notation has been assumed:

$$p=(x,y),\quad q=(\xi,\eta),\quad r=\sqrt{[(x-\xi)^2+(y-\eta)^2]},\quad r'=\sqrt{[(x-\xi)^2+(y+\eta)^2]},$$
$$R=\sqrt{[(x-\xi)^2+(\alpha+y+\eta)^2]},\quad \nu=\omega^2/g,\quad K=|\nu\cos\theta|,$$

$K_n[\ ]$ is a modified Bessel function of the second kind of nth order, θ is the wave heading and ω is the wave frequency.

In equation (1) $\phi(q)$ represents the unknown velocity potential and $v_n(q)$ is a known function representing $\partial\phi(q)/\partial n_q$ over C_w. The unit normal vector is directed into the fluid as indicated in Figure 1.

3. SOLUTION OF FREDHOLM INTEGRAL EQUATIONS

The numerical solution of integral equations is a fairly well documented topic; see, for instance, Baker[4] and Delves and Walsh.[5] Several methods are available, such as the use of direct quadrature rules, the use of the Rayleigh–Ritz and Galerkin methods or the use of the so-called expansion methods amongst others. Expansion methods, as their name suggests, represent the unknown as an expansion in terms of known base functions; that is,

$$\phi=\sum_{i=1}^{N}a_i f_i,\quad \text{say.} \tag{3}$$

The f_i are the base functions and the a_i are constants which now become the unknowns of the problem. These expansions may be defined locally or over the whole integration domain. One particular method of obtained the a_i values is the collocation method. This consists of satisfying the integral equation, equation (1), at N selected points of C_w. Thus N equations are obtained in the N unknowns which can be solved using the standard procedures of linear algebra. The collocation method is the approach used in this paper.

3.1. A particular approach

It can be easily seen that on substituting equation (3) into equation (1), the coefficients of the a_i for any of the N equations will be the integrals of the basis functions f_i times the normal derivative of the Green function. These integrals are defined over C_w which will invariably be of arbitrary form and without mathematical representation. Thus before trying to apply the method we must tackle the problem of evaluating the integrals of complicated functions over arbitrary contours. Because of the complexity of the Green function, numerical integration will inevitably have to be used. Another factor to be taken into account is that the normal vector to the contour is required as a function in the normal derivatives. All this indicates that some approximation of the contour C_w is required in order to make progress. An obvious approach would be to select a number of points on C_w and fit a curve through them using well known techniques such as cubic and B splines. This approach has been implemented in the case of a simple Rankine source in an infinite (no free surface) domain by Okan and Umpleby.[6] A second paper by these authors[7] is concerned with the

free surface effects for a steady translating 2D body. With these global curve-fitting schemes any degree of accuracy and smoothness can be achieved in the representation. Unfortunately these schemes are not trivial in terms of the computational effort regarding their implementation and their use in obtaining the required information for the integration procedure. Thus it was felt that initially a simpler approach was more desirable in approximating the contour C_w.

Without loss of generality we can divide the contour into any number of segments. Equation (1) would then become

$$\alpha\phi(p) + \sum_{j=1}^{N} \int_{C_{w_j}} \left(\phi(q) \frac{\partial G(p,q)}{\partial n_q} - G(p,q) v_n(q) \right) \mathrm{d}l_j(q) = 0. \tag{4}$$

Instead of looking for a global approximation to C_w we shall obtain local approximations within each of the N segments. The simplest approximation involves the use of the Lagrangian polynomials as pioneered in the finite element method (FEM). Thus each segment C_{w_j} will be represented in a parametric form by equations of the form

$$\left.\begin{aligned} \xi &= \sum_{i=1}^{n} \xi(q_i) N_i(t) = f(t), \\ \eta &= \sum_{i=1}^{n} \eta(q_i) N_i(t) = g(t), \end{aligned}\right\} -1 \leqslant t \leqslant 1, \tag{5}$$

where $[\xi(q_i), \eta(q_i)]$ are the co-ordinates of the ith point in the segment used to support the approximation. The number of points required, n, will depend on the order of the approximation desired; e.g., $n = 2$ for a linear function, $n = 3$ for quadratic functions, etc. The functions $N_i(t)$ are the so-called shape functions in the jargon of FEM. They are simple polynomials in the variable t of degree 1, 2 or 3 depending on whether $n = 2, 3$ or 4. Details are presented in the Appendix in conjunction with the location of the points defining the approximation in the t domain. The selected shaped functions have the property that

$$N_i(t_j) = \begin{cases} 1 & i = j, \\ 0 & i \neq j, \end{cases}$$

where t_j is the t value corresponding to the point q_j. Suppose that the mapping of the jth segment is such that as t increases from -1 to $+1$ the segment is traversed with the fluid region on the left-hand side. Then it can be easily shown that the normal vector pointing into the fluid is given by

$$\mathbf{n} = \frac{1}{\sqrt{[(f_j')^2 + (g_j')^2]}} (-g_j'\mathbf{i} + f_j'\mathbf{j}), \tag{6}$$

where f' and g' denote derivatives with respect to t. If the direction of travel along the segment were defined in the opposite direction, then the sign of the normal would simply change. It also follows that the arc length can be written as

$$\mathrm{d}l_j(q) = \sqrt{[(f_j')^2 + (g_j')^2]}\, \mathrm{d}t. \tag{7}$$

Therefore by means of the representation defined by equation (5), the integrals over the segments making up C_w have been mapped to the $[-1, 1]$ segment of the real t axis. This means that we can now apply Gaussian quadrature in a straightforward manner except for the singular cases discussed later.

With this representation of the geometry it is obvious that no slope continuity can be ensured across neighbouring segments. Thus a jump in the normal unit vector exists at these points. This

poses no mathematical difficulty as functions with finite discontinuities or jumps have well defined integrals. In implementing the direct method of solution, the actual value of the normal at such intersection points is not required provided a suitable quadrature rule is chosen, such as Gaussian quadrature. Since the normal vector is part of the integrand, then each facet will have its own well defined normal in the neighbourhood of these points.

Next, using equations (6) and (7) and the fact that

$$\partial/\partial n = \mathbf{n}\cdot\nabla \quad \text{and} \quad v_n = \mathbf{n}\cdot[\mathbf{i}v_x + \mathbf{j}v_y],$$

equation (4) can be rewritten as

$$\alpha\phi(p) + \sum_{j=1}^{N} \int_{-1}^{+1} \phi(q)\left(-g_j'(t)\frac{\partial G(p,q)}{\partial \xi} + f_j'(t)\frac{\partial G(p,q)}{\partial \eta}\right) \mathrm{d}t$$
$$- \sum_{j=1}^{N} \int_{-1}^{+1} G(p,q)\left(-g_j'(t)v_x + f_j'(t)v_y\right) \mathrm{d}t = 0, \tag{8}$$

where p is a fixed point and the co-ordinates of q are given by equation (5). In order to obtain a true set of simultaneous equations from equation (8), we now need to introduce the approximation for ϕ over the segments. Here we follow the same technique used in the FEM and express the potential as

$$\phi = \sum_{k=1}^{m} \phi(q_k) M_k(t), \tag{9}$$

where the $M_k(t)$ are the same shape functions defined in the Appendix for the representation of the geometry. The unknown $\phi(q_k)$ are the values of ϕ at the points q_k dictated by the specification of m over the segment. That is, the location of these points on the segment, as a function of t, is as for the geometric case. Here we have used m and M_k instead of n and N_i to indicate that different orders of representation can be used for the geometry and the unknown function. The values of m permitted are the same as for n except that now we also have the choice of $m = 1$ to indicate a constant approximation of the dependant variable ϕ.

Hess[8] presented a different approach for the use of higher-order approximations in the solution of his two-dimensional aerodynamic boundary value problems. In the development of his method Hess comes to the conclusion that a mathematically consistant formulation requires the order of approximation for the unknown function to be one less than that of the geometry of a given segment. The authors have studied Hess's procedure in detail and find they are unable to fully agree with the criteria and arguments leading to the aforementioned conclusions.

The Hess viewpoint on the relationship between the two orders of approximation is not shared by the wide FEM community, where isoparametric elements are commonly used. In fact Brebbia *et al.*[9] argue that the order of approximation of the unknown must be at least the same as that of the geometry. This conclusion is based on the FEM argument that the approximation used in terms of the local co-ordinates (t) must be able to reproduce a complete polynomial, in the global co-ordinates of the problem, of the first degree at least. This is required because in FEM problems in general the unknown and its first derivatives are present under the integral sign, thus requiring a complete polynomial of order one to ensure convergence.[10]

In our particular case only the unknown itself appears under the integral sign, so that the above requirement of an isoparametric element appears rather restrictive. This view is supported by the extensive use and good results provided by the well tried linear–constant formulation, which under the above rules would be invalid!

Hence substituting equation (9) in equation (8), the set of simultaneous equations is defined by

$$\alpha\phi(p_i) + \sum_{j=1}^{N}\left[\sum_{k=1}^{m}\phi(q_k)\int_{-1}^{+1} M_k(t)\left(-g'_j(t)\frac{\partial G(p_i,q)}{\partial\xi} + f'_j(t)\frac{\partial G(p_i,q)}{\partial\eta}\right)\mathrm{d}t\right]$$
$$= \sum_{j=1}^{N}\int_{-1}^{+1} G(p_i,q)[-g'_j(t)v_x + f'_j(t)v_y]\,\mathrm{d}t, \tag{10}$$

for $i = 1$ to M. The p_i are the M distinct points used to define the approximation of the velocity potential. Obviously when p_i is a point at the intersection of two elements, then it will support the local approximation of ϕ on both elements. Hence $M = N$ for the case of constant approximation and $M = N(m-1)+1$ for higher-order approximations.

It must be noted that in equation (10) ϕ, G, v_x and v_y are all complex quantities, so that equation (10) is in fact a set of complex simultaneous equations. Once the relevant matrices have been set up, then the system can be solved in the traditional way. The required integrals are all evaluated numerically using Gaussian quadrature.

For the diffraction boundary value problem, the velocity components are defined as

$$v_x = -\partial\phi_I/\partial x \quad \text{and} \quad v_y = -\partial\phi_I/\partial y,$$

where ϕ_I is the incident wave velocity potential. For the radiation boundary value problem the x and y components of the velocity of a given point of C_w when the section performs unit amplitude oscillations in each of the degrees of freedom are

$$\begin{aligned}
&v_x = -\mathrm{i}\omega, && v_y = 0 \quad \text{for sway,}\\
&v_x = 0, && v_y = -\mathrm{i}\omega \quad \text{for heave,}\\
&v_x = \mathrm{i}\omega[g_j(t) - y_c], && v_y = -\mathrm{i}\omega[f_j(t) - x_c] \quad \text{for roll,}
\end{aligned}$$

where (x_c, y_c) are the co-ordinates of the centre of rotation.

3.2. *The hydrodynamic coefficients*

Of interest in practical calculations are the added mass and fluid damping coefficients and the exciting forces and moments. The sectional added mass and fluid damping coefficients are defined as

$$a_{rs} = \frac{\rho}{\omega}\int_{C_w}\phi_I^r n_s\,\mathrm{d}l \quad \text{and} \quad b_{rs} = -\rho\int_{C_w}\phi_R^r n_s\,\mathrm{d}l,$$

with $r, s = 2, 3$ and 4 denoting sway, heave and roll respectively. The subscripts R and I denote the real and imaginary components of the complex velocity potential and the direction cosines n_s are defined as

$$n_2 \sim n_x, \quad n_3 \sim n_y \quad \text{and} \quad n_4 \sim n_y(x - x_c) - n_x(y - y_c).$$

Using the indicated subdivision of C_w and the approximation for ϕ over each segment, the expressions for the coefficients can be re-expressed as

$$\left.\begin{aligned}
a_{rs} &= \frac{\rho}{\omega}\sum_{j=1}^{N}\int_{-1}^{+1}\left(\sum_{k=1}^{m}\phi_I^r(q_k)M_k(t)\right)n_{s_j}\,\mathrm{d}t,\\
b_{rs} &= -\rho\sum_{j=1}^{N}\int_{-1}^{+1}\left(\sum_{k=1}^{m}\phi_R^r(q_k)M_k(t)\right)n_{s_j}\,\mathrm{d}t,
\end{aligned}\right\} \quad r, s = 2, 3, 4,$$

assuming unit displacement of the section in each mode. The corresponding exciting forces and

moments are given by the expression

$$F_{E_s} = i\omega\rho \sum_{j=1}^{N} \int_{-1}^{+1} \left[\left(\sum_{k=1}^{m} \phi_D(q_k) M_k(t) \right) + \phi_I \right] n_{s_j} \, dt \, e^{-i\omega t},$$

for $s = 2, 3, 4$, where ϕ_D and ϕ_I are the complex diffraction and incident wave velocity potentials respectively. In each case the n_s values on a particular facet j are given by

$$n_{2_j} \sim -g'_j(t), \quad n_{3_j} \sim f'_j(t), \quad n_{4_j} \sim f'_j(t)[f_j(t) - x_c] + g'_j(t)[g_j(t) - y_c].$$

4. IMPLEMENTATION OF THE PROCEDURE

In the previous section of this paper we derived equation (10). Application of this equation at each of the selected points where $\phi(q_k)$ is to be determined leads to a set of complex linear simultaneous equations for the unknowns $\phi(q)$. We can write these equations in matrix form as

$$(\mathbf{A} + i\mathbf{B})(\boldsymbol{\phi}_R + i\boldsymbol{\phi}_I) = \mathbf{C} + i\mathbf{D},$$

where **A** and **B** are $M \times M$ matrices and $\boldsymbol{\phi}_R, \boldsymbol{\phi}_I$, **C** and **D** are $M \times 1$ column vectors, all being real. Obviously for each of the radiation and diffraction problems defined earlier there will correspond different **C** and **D** vectors, while **A** and **B** will be the same for all problems of specified frequency. Thus in practice **C** and **D** are $M \times$ nprob real matrices, where nprob is the number of problems considered together at any one time.

The elements of the matrices **A**, **B**, **C** and **D** are made up by the values of the integrals indicated in equation (10) over the relevant facets. Recalling that the Green function G is of the form $G = G_R + iG_I$, it follows that the elements of **A** will be a linear combination of terms of the form

$$\int_{-1}^{+1} M_k(t) \left(-g'_j(t) \frac{\partial G_R}{\partial \xi} + f'_j(t) \frac{\partial G_R}{\partial \eta} \right) dt$$

and the elements of **B** a combination of terms of the form

$$\int_{-1}^{+1} M_k(t) \left(-g'_j(t) \frac{\partial G_I}{\partial \xi} + f'_j(t) \frac{\partial G_I}{\partial \eta} \right) dt.$$

Since the velocity components v_x and v_y are complex quantities of the form

$$v = v_R + iv_I,$$

then the elements of the **C** column vector are of the form

$$\sum_{j=1}^{N} \int_{-1}^{+1} [G_R(p_i, q) v_{R_j} - G_I(p_i, q) v_{I_j}] \, dt$$

and those of the **D** column vector are of the form

$$\sum_{j=1}^{N} \int_{-1}^{+1} [G_R(p_i, q) v_{I_j} + G_I(p_i, q) v_{R_j}] \, dt,$$

where

$$v_{R_j} = -g'_j(t) v_{x_R} + f'_j(t) v_{y_R}$$

and

$$v_{I_j} = -g'_j(t) v_{x_I} + f'_j(t) v_{y_I}.$$

Thus it can be seen that one of the most important and time-consuming aspects of the method is the accurate evaluation of these integrals. The imaginary part of the Green Function, G_I, is a well behaved function which is nowhere singular. Thus the evaluation of the elements of the **B** matrix can be undertaken using straightforward numerical integration in all cases. The same applies to the integration of those parts involving G_I for the elements of the **C** and **D** vectors.

The real part of the Green function and its derivatives exhibit a singular behaviour when the field point p and the integration variable point q coincide. The singular behaviour of the Green function arises from the presence of the $\ln r$ terms and their derivatives. The $\ln r$ singularities are handled using the Lean and Wexler[11] quadrature procedure, whereas the singularities associated with the derivatives can be shown to be non-singular in the limit and hence integrated using any standard numerical integration procedure which does not explicitly involve the singular point.

4.1. Numerical integration

All integrals which are free of any form of singularity are evaluated using Gauss–Legendre quadrature, whose weights and ordinates are given by Stroud and Secrest.[12] This quadrature rule is exact for polynomials of degree $\leqslant 2n-1$, where n is the number of ordinates.

In practice the accuracy of the integral is controlled by evaluating the integral with an increasing number of ordinates. In fact, if we denote the value of the integral evaluated with n ordinates by I_n, then for the calculations presented in this paper the iterative process is stopped when

$$\left|\frac{I_n - I_{n+2}}{I_n}\right| \leqslant 0{\cdot}001.$$

That is, when the relative change is less than or equal to 0·1%. With Gaussian quadrature this process is rather wasteful since the ordinates for any two values of n are not the same. Thus a substantial number of integrand evaluations go unused in the final result.

An attempt to alleviate this situation was made by Patterson,[13] who developed a Gaussian-based rule which enabled the number of ordinates to be increased by $n+1$ values while retaining the integrand evaluation for previously used ordinate values. The rule commences with the three-point Gauss–Legendre rule, and further weights and ordinates have been evaluated for $n = 7, 15, 31, 63, 127$ and 225. One slight disadvantage is that while the ordinates from the previous n value can be used again, new weights must be applied to the function every time. This clearly requires the storage of all previous integrand evaluations.

In practice it was found that the total number of integrand evaluations, using the same relative error criteria defined above, was in most cases larger than using the standard Gauss–Legendre scheme. This is as a result of two facts. In the first place, as the iteration proceeds the number of ordinates increases quite rapidly. Secondly, because of the substantial jump in the number of ordinates from one iteration to the next, the relative error is bound to be substantial compared with that obtained from a more moderate and steady increase in the number of ordinates. These two factors conspire to make the iteration reach quite high values of n before the relative difference criteria is satisfied, thus negating any benefit accrued from not throwing away any integrand evaluation.

5. ASSESSMENT OF THE HOBE METHOD

The performance of the HOBE method can be assessed chiefly in two ways: on the grounds of accuracy of the solution or on the grounds of computer central processor unit (CPU) time. The

main impetus for researching higher-order boundary element formulations is the achievement of greater accuracy for a given number of facets or a reduction in the CPU time for a given accuracy with fewer facets, all assessments being made in relation to the standard linear–constant procedure.

The question of assessment in terms of accuracy is rather easy to establish, since we can use the standard method with a very fine discretization as a basis for comparison. The comparison can be carried out at two levels. We can compare the distribution of the velocity potential over the contour of the cross-section or we can compare the value of the relevant hydrodynamic coefficients. Naturally the former comparison is the more stringent of the two, since the integral nature of the evaluation process for the coefficients will tend to reduce considerably any discrepancies in the distribution of the potential over the section.

The question of CPU time is rather more subtle as this involves such aspects as the efficient implementation of the method in the form of a computer program and the selection of suitable numerical algorithms. Thus, inevitably, this involves the ability and experience of the programmer. Hence this is a rather subjective quantity even if the comparison is carried out in the same computational environment.

In general it is possible to obtain the same accuracy as the base method with a reduced number of higher-order facets. Since this reduces the order of the linear algebraic problem, it is obvious that substantial savings in solution CPU time will accrue, because this time varies as M^3. That is, halving the number of collocation points M results in the time being reduced by a factor of eight. However, because of the greater complexity of the formulation and the required use of numerical integration, the CPU time required to formulate the linear algebraic problem will increase. It is when we consider the set-up time in particular that the HOBE exhibits an unfavourable handicap when compared with the standard linear–constant method.

Let us digress slightly and consider some of the details of the practical implementation of the standard method. In spite of having assumed a constant value of the unknown over the linear facet, we still have to evaluate the integrals of the normal derivative of the Green function for matrices **A** and **B**, and of the Green function times the normal velocities for the **C** and **D** matrices. For problems governed by Laplace's equation, integrals of the Green function and its normal derivative can be evaluated analytically over linear facets by using complex variables and integration in the complex plane.[2] For the integrals of the **C** and **D** matrices this requires the further assumption that the normal velocity is constant over the facet and can therefore be taken outside the integral sign.

Analytic integration results in rather complicated expressions which are somewhat time-consuming to evaluate. For this reason it is far more common in practical programs to use the mid-point rule. This means that the integrals are approximated by the product of the value of the integrand at the facet mid-point and facet length. This approach is quite satisfactory from a practical engineering point of view provided the number of facets is not too low. In any case the main advantage is that a substantial reduction of the set-up time is achieved. This follows because of the much simpler expressions to be evaluated and because the reciprocity properties of the Green function can be exploited so as to halve the number of quantities to be evaluated. This is true even when symmetry properties are taken into account.

To illustrate this point let us consider a typical problem where there is no symmetry of the solution. In this case the elements of the matrices, **A** and **B** in particular, represent the influence of a given facet at a given collocation point. For instance, the element $A(i,j)$ of **A** represents the influence of the jth facet on the ith collocation point, which is situated somewhere on the ith facet. The element $A(j,i)$ has a similar meaning. If we denote the collocation points associated with the ith and jth facet by p_i and p_j, then we know that $G(p_i, p_j) = G(p_j, p_i)$. When considering the normal derivative $\partial G/\partial n_q$, things are not as straightforward. But it can be easily shown that $\partial G/(p_i, p_j)/\partial n_{q_j}$

and $\partial G(p_j, p_i)/\partial n_{q_i}$ can be obtained from a single evaluation of $\partial G/\partial \xi$ and $\partial G/\partial \eta$. Thus for a problem with N facets we only need to evaluate the Green function and its derivatives a total of $N(N+1)/2$ times.

If the integrals are to be evaluated analytically or otherwise, none of the above properties of the Green function can be used, even for the traditional linear–constant elements. Hence by actually attempting to evaluate the integrals, the set-up time increases by a factor of at least two. If in addition we use higher-order elements where there are more integrals with more complicated integrands, the time will increase quite considerably. For these reasons any time comparison of the HOBE method with a standard method using the mid-point rule gives the latter a rather unfair advantage. This means that only an extremely efficient computer program of the HOBE method will have a good chance of competing favourably against the standard methods as far as CPU time is concerned. The above arguments should be borne in mind when studying the time comparisons to be presented.

6. APPLICATION OF THE HOBE METHOD

The availability of curved facets in the HOBE method should be exploited first of all to achieve the best possible geometric approximation of the section. In spite of the unavoidable slope discontinuities at facet boundaries, this can be achieved by judicious distribution of facets so as to maximize the curvature properties of the facets. For instance, a quadratic facet cannot handle changes in the sign of the curvature within the facet so that the representation will only be an arc passing through the three points defining the facet. On the other hand, a cubic facet can have a point of inflection within the facet and can therefore be used to cover larger distances. In this way the extent of slope discontinuity can be reduced quite considerably.

A good representation of the section is important since the boundary conditions of the problems of interest are heavily dependent on the geometric properties of the section. This is particularly important for the direct method of solution where the boundary conditions appear in the integrand of the right-hand side of the integral equation. Thus the number of facets used in the discretization should be controlled by the need for good geometric representation. It should be noted that unlike the standard case, the number of equations and unknowns is given by the total number of collocation points M and not the number of facets N. The value of M, for a given number of facets, can be controlled by the order of approximation selected for the unknown on every facet. In any case the number of facets required is substantially less with the HOBE method than with the standard model.

Thus after having fixed the number of facets according to the criteria described above, a suitable order of approximation for the unknown function has to be selected. This selection is a rather subjective matter and must rely to a large extent on experience gained from extensive usage of the HOBE method. It will obviously depend on whether the motivation for the application is time or accuracy. If a time reduction is being sought, then the order of approximation should be such as to keep the number of collocation points low without overstretching the approximation of the velocity potential. It seems that acceptable engineering results will be obtained provided the number of collocation points does not fall too far below half the number that would be normally used for the standard method. More specific points in this respect will be brought out when discussing the results for each of the sections analysed.

6.1. Specific 2D sections analysed

Application of the HOBE method is illustrated through analysis of two ship aft sections and the

transverse section through the submerged pontoons of a semi-submersible. Each aft section selected exhibits a substantial degree of curvature, whereas the pontoons are of rectangular cross-section with differing corner radii. The geometric discretization of each ship section, denoted by the letters A and B, is shown in Figures 2 and 3. The figures indicate the fit achieved by the discretization and also include the normal vector at selected points of the facet to indicate the degree of smoothness achieved at the junction of two neighbouring facets. For both sections five cubic and seven quadratic facets have been used in Figures 2(a), 3(a) and Figures 2(b), 3(b) respectively.

The cross-section of each of the semi-submersible pontoons has a depth of 8·0 m and a width of 16·0 m, with the pontoons' centre lines being 60·94 m apart. Pontoon corner radii of 1·0 m and 4·0 m will be considered with 16 and 6 quadratic facets respectively as shown in Figures 4(a) and 4(b).

6.2. *Specific problems investigated*

Each of the 2D sections described has been analysed to solve the radiation problems of sway, heave and roll and the diffraction problem for various wave headings and wave frequencies. Since the results for the diffraction analysis for headings different to beam sea will not add or subtract anything from our conclusions, only results for beam seas are presented in this paper.

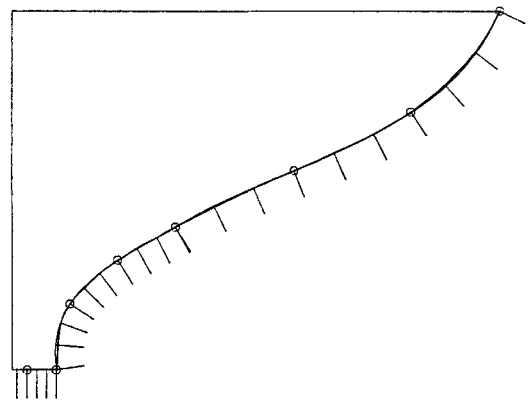

Figure 2(a). Piece-wise cubic approximation with 5 facets (section A); beam = 13·20 m, draught = 4·78 m

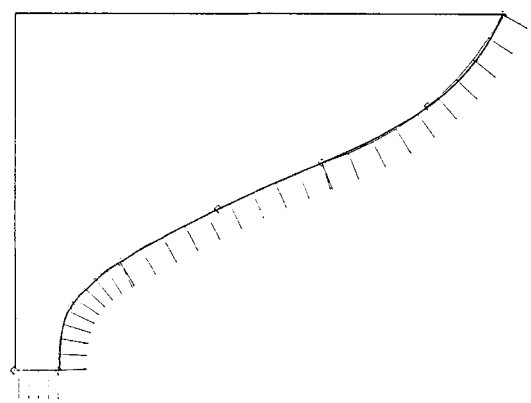

Figure 2(b). Piece-wise quadratic approximation with 7 facets (section A); beam = 13·20 m, draught = 4·78 m

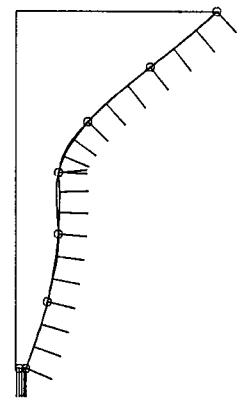

Figure 3(a). Piece-wise cubic approximation with 5 facets (section B); beam = 11·20 m, draught = 9·82 m

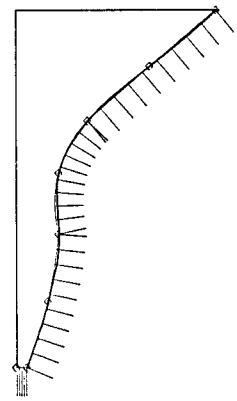

Figure 3(b). Piece-wise quadratic approximation with 7 facets (section B); beam = 11·20 m, draught = 9·82 m

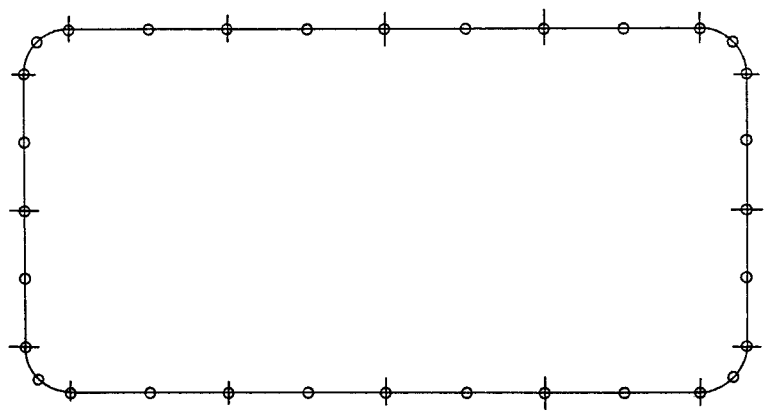

Figure 4(a). Piece-wise quadratic approximation with 16 facets (semi-submersible pontoons section, survival draught); corner radius = 1·0 m

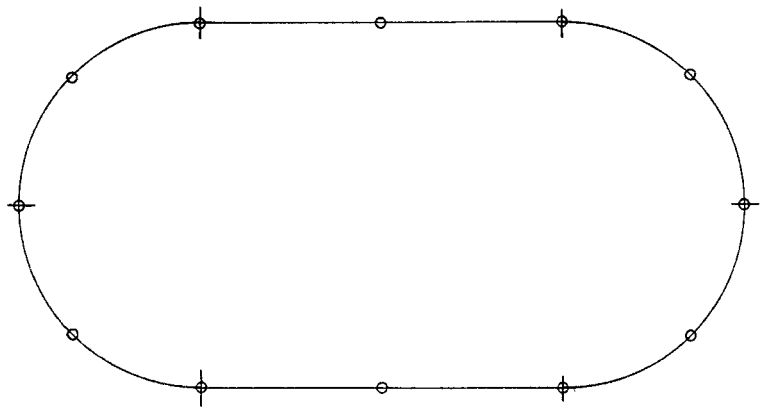

Figure 4(b). Piece-wise quadratic approximation with 6 facets (semi-submersible pontoons section, survival draught); corner radius = 4·0 m

6.3. *Results presented*

The results obtained from the analysis described in Section 6.2 are as follows:

(a) plots of added mass coefficients, fluid damping coefficients and amplitude and phase of exciting force/moments over range of $\omega^2 B/2g$ values from 0·1 to 6·0 for the ship sections, and over a range of wave periods from 2 to 20 s for the semi-submersible pontoon section;
(b) plots indicating the variation over the contour of the in-phase and out-of-phase components of the velocity potentials for $\omega^2 B/2g$ values of 0·1, 1·0, 2·0, 4·0 and 6·0;
(c) table showing the CPU time comparisons between the different HOBE models used and the standard Frank close-fit method.

For obvious reasons of space, only those results which show the more salient features of the method or serve to highlight particular points will actually be presented in the paper.

In the results presented, the velocity potentials are not non-dimensionalized whereas the reactive hydrodynamic coefficients and roll excitation forces are non-dimensionalized by division by the following indicated factors:

$$\begin{array}{llll} a_{22}, & a_{33} & \text{by} & \rho B^2, \\ b_{22}, & b_{33} & \text{by} & \rho B^2/\sqrt{(B/g)}, \\ a_{44} & & \text{by} & \rho B^4, \\ b_{44} & & \text{by} & \rho B^4/\sqrt{(B/g)}, \\ f_4 & & \text{by} & \rho g B^2 a, \end{array}$$

where B is the waterline beam of the section for sections A and B and corresponds to the beam of the semi-submersible measured to the outer sides of the pontoons, and a is the wave amplitude.

6.4. *Discussion of results*

6.4.1. Sectional hydrodynamic coefficients. Because of the range of frequencies covered by the analysis for the ship sections, the first irregular frequencies are included within this range. In general, the results indicate that the HOBE results are affected by the irregular frequencies to a greater extent than is the case for the Frank close-fit method. This is particularly the case for

discretizations with a low order of approximation for the potential, which indicates that the irregular frequencies problem is aggravated by the low number of collocation points.

Since the semi-submersible pontoon section is totally submerged, no irregular frequencies exist, but the interference effects between the two pontoons can be clearly seen over the range of periods from 5 to 10 s. The distance between the pontoon centre lines is 60·94 m, which for the case of infinite depth corresponds to a wave of 6·25 s period. Therefore the highly oscillatory behaviour of the hydrodynamic coefficients can almost certainly be attributed to the presence of resonance phenomena.

For section A we present the reactive hydrodynamic coefficients for sway, heave and roll in Figures 5, 6 and 7 respectively and the roll exciting moment in Figure 8. The agreement between all HOBE discretizations and the standard Frank close-fit method up to the first irregular frequency is very good. Beyond the first irregular frequency only the discretizations with quadratic and cubic approximations for the potential exhibit a reasonable performance, though as already indicated they are more severely affected than the Frank close-fit results. The discretizations with a linear approximation perform rather badly throughout the frequency range except at very low frequencies.

For section B we only present the reactive coefficients and exciting moment for roll in Figures 9 and 10 respectively, since the results for the other coefficients show the same trends as in the case of section A. In the case of the roll degree of freedom, it can be seen that only HOBE discretizations with a cubic approximation of the potential give results which are close to those from the Frank close-fit method. This abnormal behaviour for the roll results can probably be attributed to the T shape of the section (see Figure 3), which would make roll-related quantities quite sensitive to the discretization used.

For the semi-submersible pontoon section, only the sway reactive coefficients and the roll exciting moment are presented, in Figures 11 and 12 respectively for a corner radius of 1·0 m and in Figures 13 and 14 respectively for a corner radius of 4·0 m. The HOBE results have been compared with those from the standard linear–constant approach based on analytic integration, with both a very fine discretization and a discretization consistent with that used for 'practical' calculations. For a corner radius of 1·0 m all the results are very close throughout the period range. For a corner radius of 4·0 m the HOBE results with a linear approximation of the potential show substantial discrepancies. In this case it should be noted that the number of facets in the HOBE discretization is just over a quarter of that used for the standard method, whereas for the case of a 1·0 m corner radius the number in the HOBE method was just under a half of that used in the standard calculation. This difference arises because the greater curvature of the section when the corner radius is 4·0 m allows the use of fewer and longer facets. When the corner radius is only 1·0 m, the quadratic facets covering the curved region are rather short and as a result more facets of moderate length over the straight portions of the section are required. Therefore a discretization with a linear approximation of the potential in the case of a corner radius of 4·0 m is much more coarse than the equivalent discretization in the case of corner radius of 1·0 m.

6.4.2. Velocity potential distribution. Plots of selected velocity potentials against the angular polar co-ordinates of points on the contour are presented in Figures 15–18 for the ship sections only. In these plots the symbols indicate the value of the potential at collocation points as determined by the calculation procedure.

The velocity potential curves are obtained by determining the value of the potential at ten points which are equidistant in the 't' domain; then one of the curve-fitting routines provided by an available graphics package is used to draw a curve passing through these points.

For section A we present the roll and diffraction velocity potential distributions in Figures 15

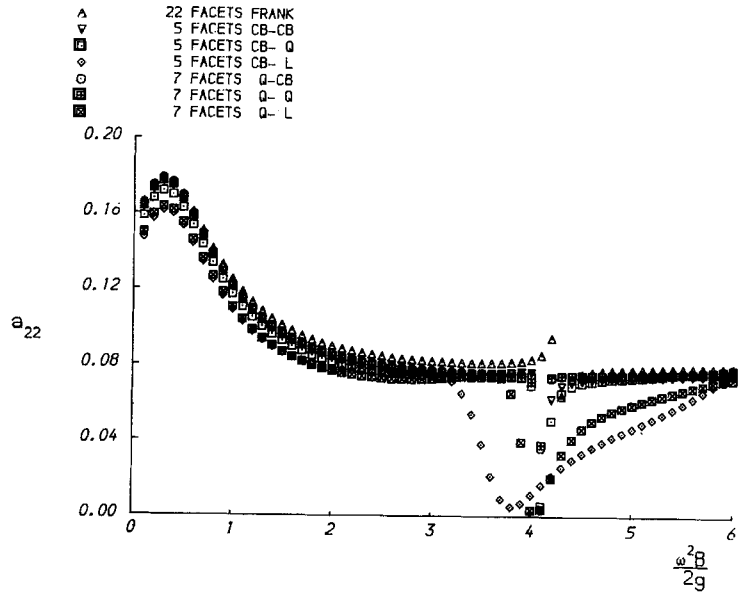

Figure 5(a). 2D sway added mass coefficient (section A); beam = 13·20 m, beam/draught = 2·76, sectional area coefficient = 0·48

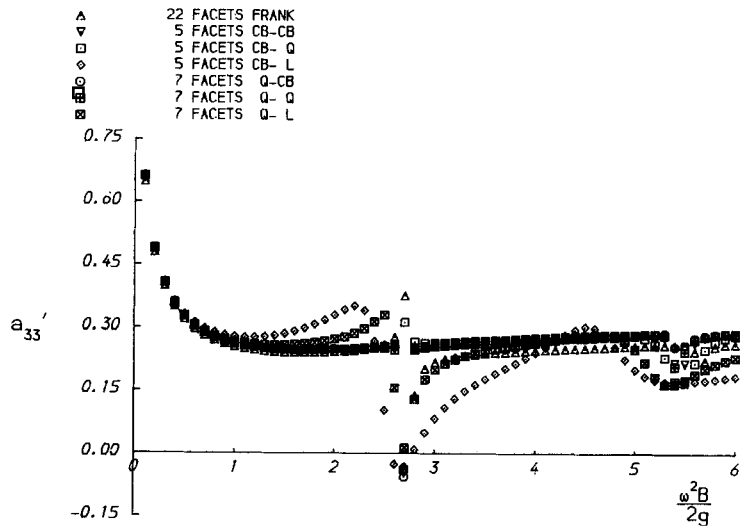

Figure 6(a). 2D heave added mass coefficient (section A); beam = 13·20 m, beam/draught = 2·76, sectional area coefficient = 0·48

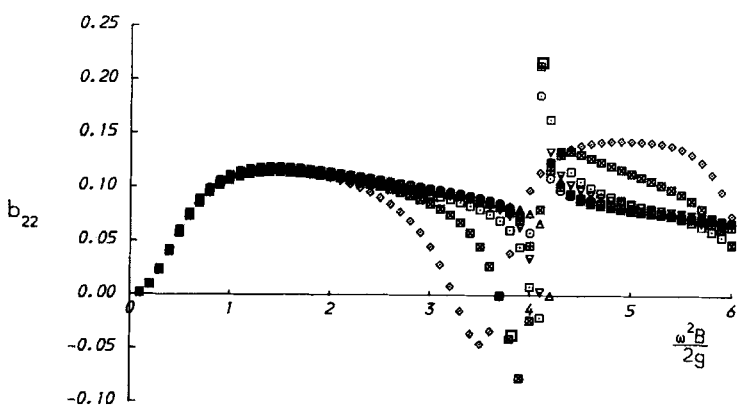

Figure 5(b). 2D sway fluid damping coefficient (section A); beam = 13·20 m, beam/draught = 2·76, sectional area coefficient = 0·48

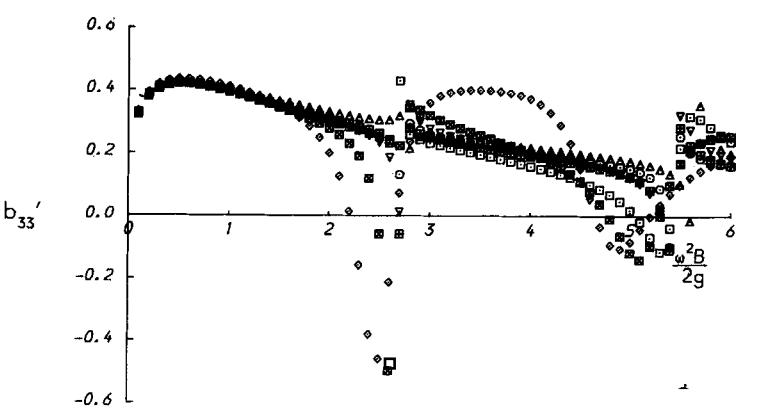

Figure 6(b). 2D heave fluid damping coefficient (section A); beam = 13·20 m, beam/draught = 2·76, sectional area coefficient = 0·48

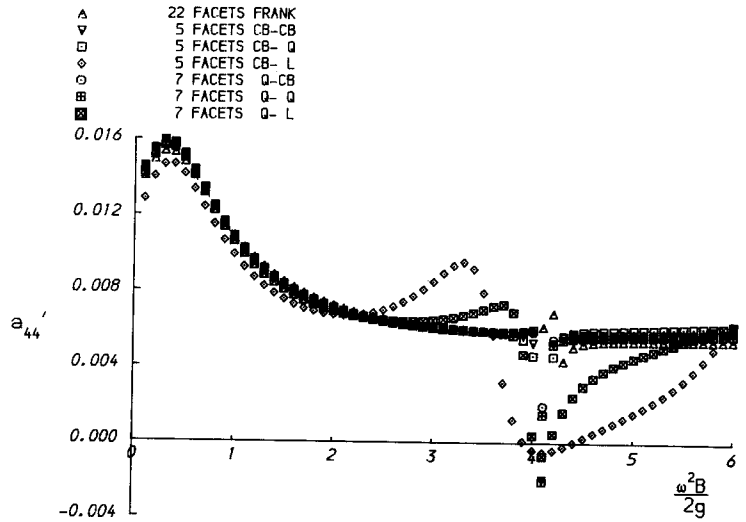

Figure 7(a). 2D roll added inertia coefficient (section A); beam = 13·20 m, beam/draught = 2·76, sectional area coefficient = 0·48

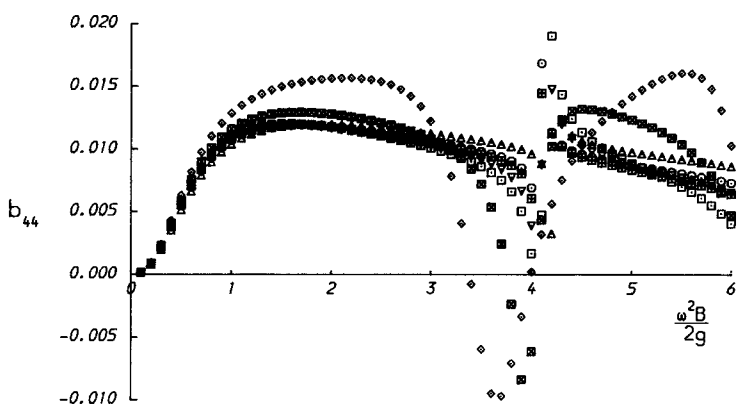

Figure 7(b). 2D roll fluid damping coefficient (section A); beam = 13·20 m, beam/draught = 2·76, sectional area coefficient = 0·48

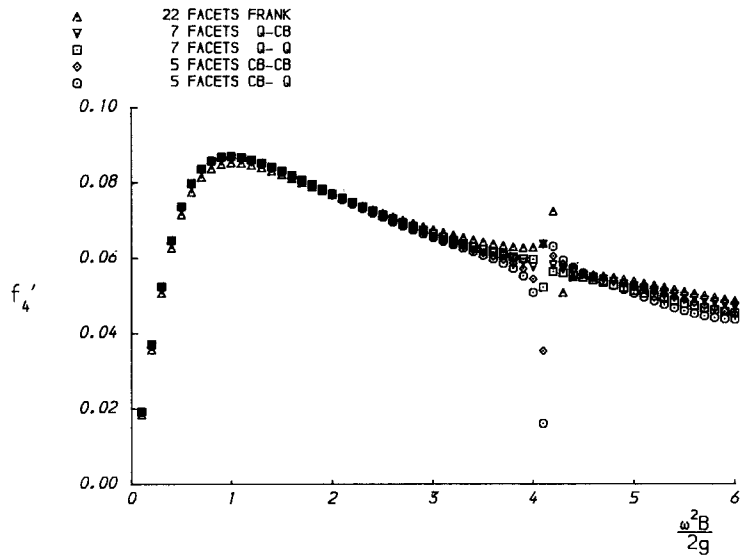

Figure 8(a). 2D roll exciting moment amplitude (section A); beam = 13·20 m, beam/draught = 2·76, sectional area coefficient = 0·48, beam sea

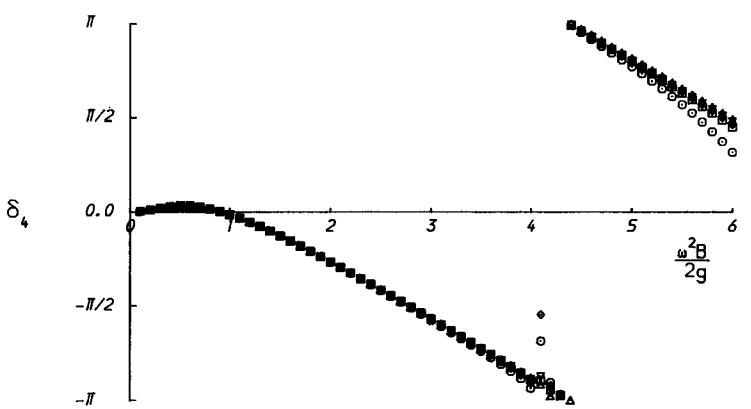

Figure 8(b). 2D roll exciting moment phase angle (section A); beam = 13·20 m, beam/draught = 2·76, sectional area coefficient = 0·48, beam sea

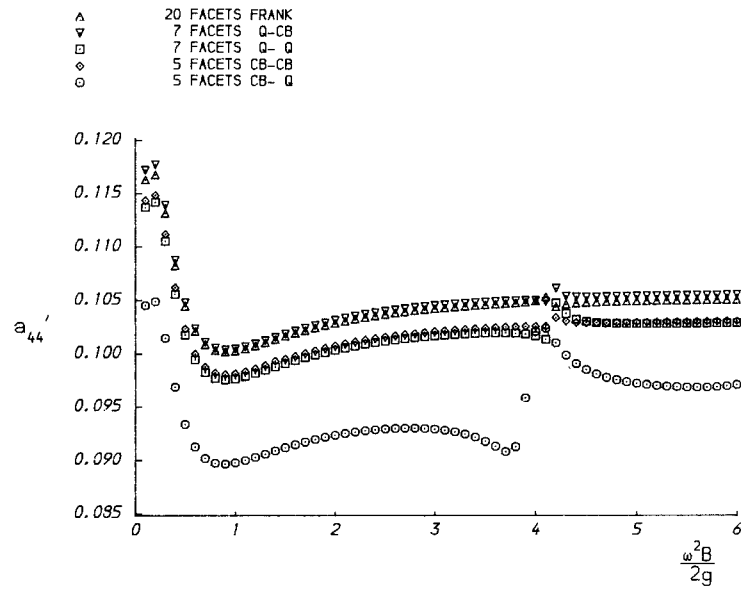

Figure 9(a). 2D roll added inertia coefficient (section B); beam = 11·20 m, beam/draught = 1·14, sectional area coefficient = 0·34

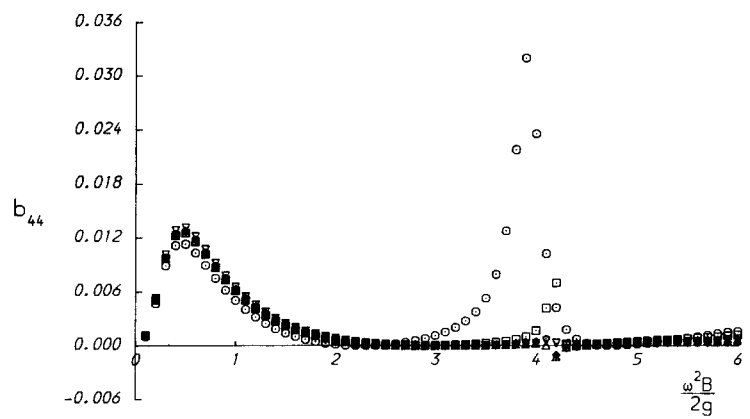

Figure 9(b). 2D roll fluid damping coefficient (section B); beam = 11·20 m, beam/draught = 1·14, sectional area coefficient = 0·34

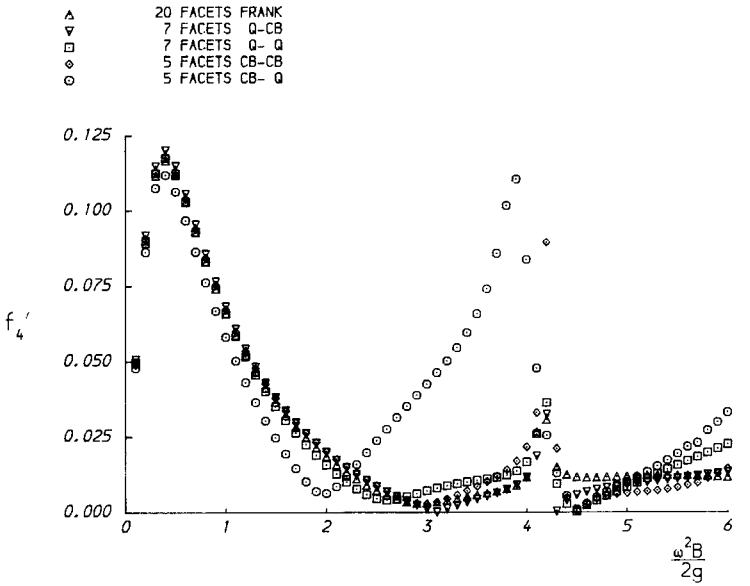

Figure 10(a). 2D roll exciting moment amplitude (section B); beam = 11·20 m, beam/draught = 1·14, sectional area coefficient = 0·34, beam sea

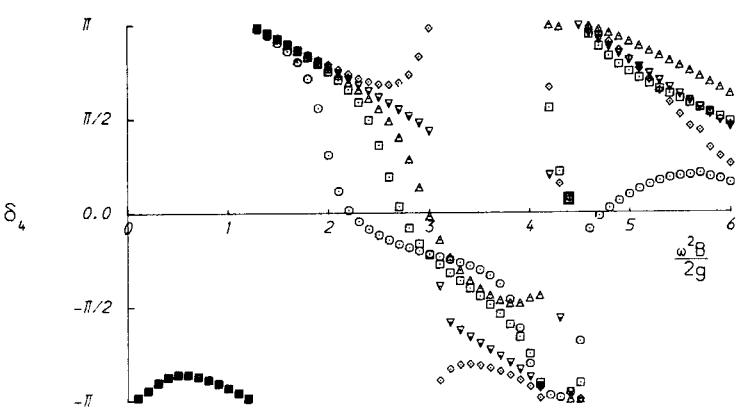

Figure 10(b). 2D roll exciting moment phase angle (section B); beam = 11·20 m, beam/draught = 1·14, sectional area coefficient = 0·34, beam sea

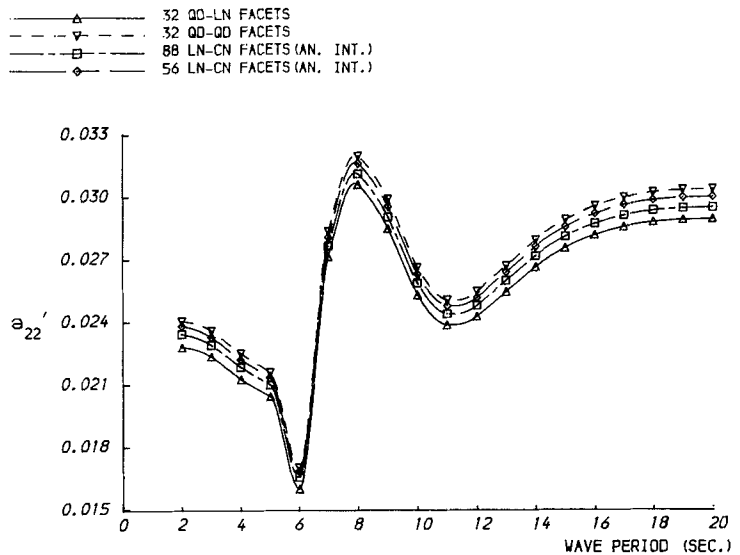

Figure 11(a). 2D sway added mass coefficient (semi-submersible pontoons section, survival draught); corner radius = 1·00 m, infinite depth

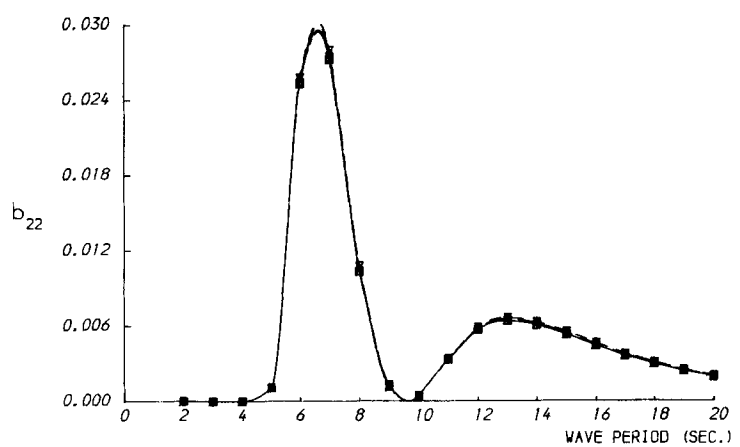

Figure 11(b). 2D sway fluid damping coefficient (semi-submersible pontoons section, survival draught); corner radius = 1·00 m, infinite depth

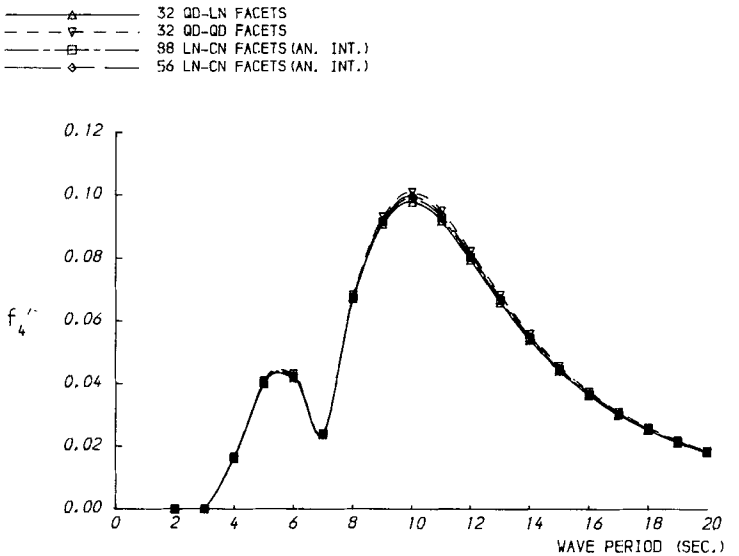

Figure 12(a). 2D roll exciting moment amplitude (semi-submersible pontoons section, survival draught); corner radius = 1·00 m, infinite depth, beam sea

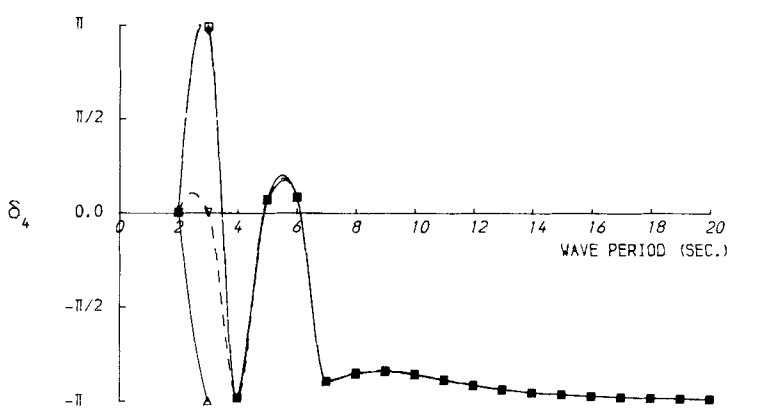

Figure 12(b). 2D roll exciting moment phase angle; corner radius = 1·00 m, infinite depth, beam sea

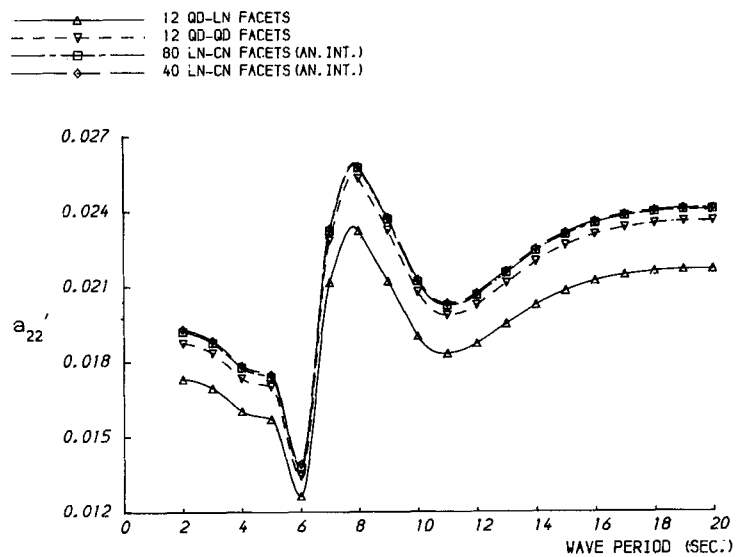

Figure 13(a). 2D sway added mass coefficient (semi-submersible pontoons section, survival draught); corner radius = 4·00 m, infinite depth

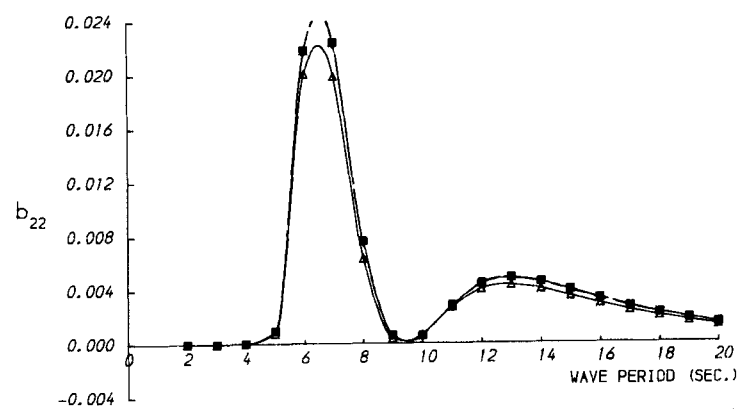

Figure 13(b). 2D sway fluid damping coefficient (semi-submersible pontoons section, survival draught); corner radius = 4·00 m, infinite depth

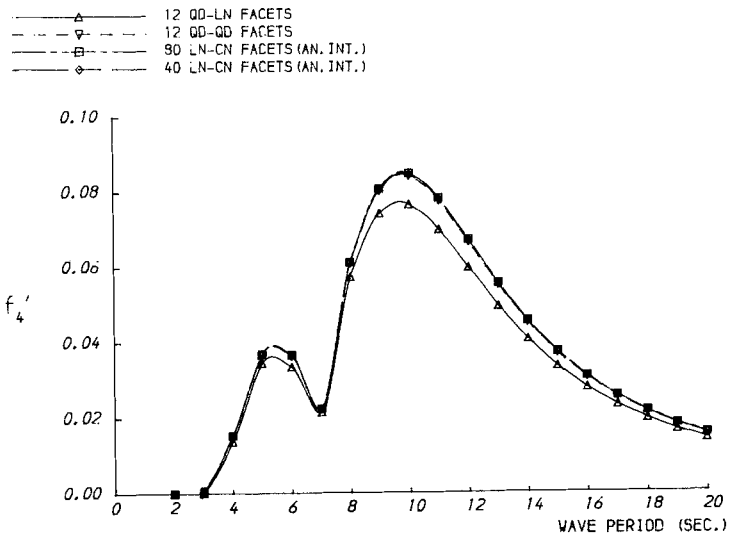

Figure 14(a). 2D roll exciting moment amplitude (semi-submersible pontoons section, survival draught); corner radius = 4·00 m, infinite depth, beam sea

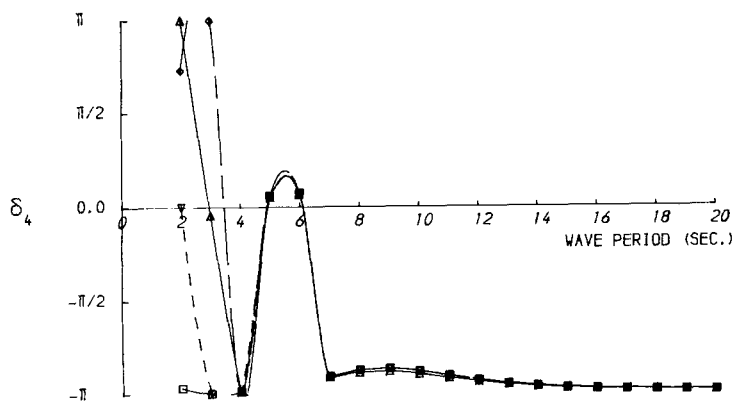

Figure 14(b). 2D roll exciting moment phase angle (semi-submersible pontoons section, survival draught); corner radius = 4·00 m, infinite depth, beam sea

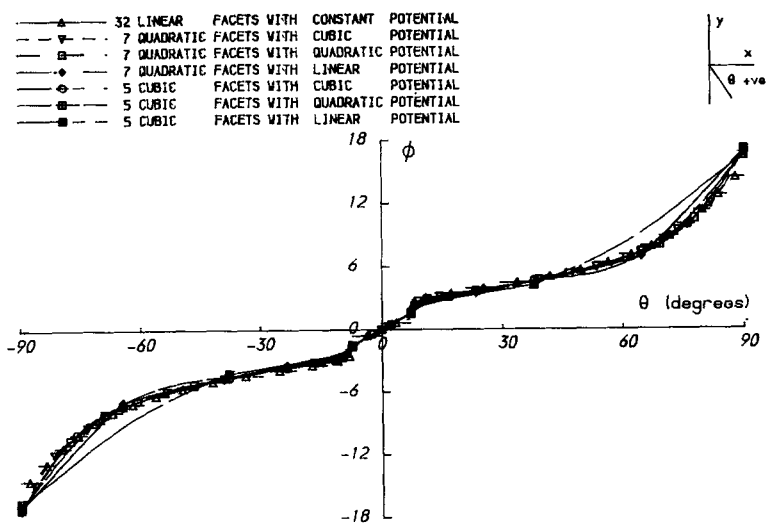

Figure 15(a). In-phase roll velocity potential (section A); $\omega^2 B/2g = 1{\cdot}00$

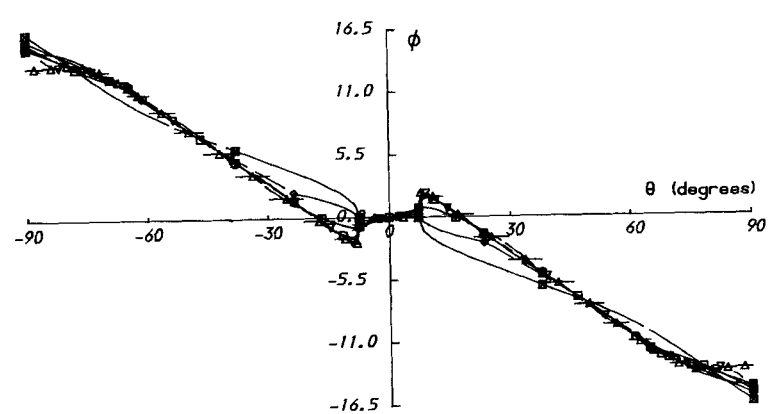

Figure 15(b). Out-of-phase roll velocity potential (section A); $\omega^2 B/2g = 1{\cdot}00$

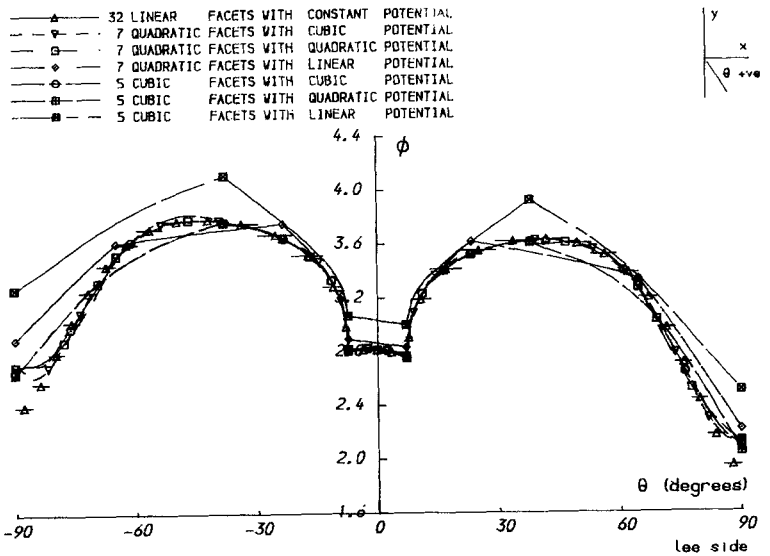

Figure 16(a). In-phase diffraction velocity potential (section A); $\omega^2 B/2g = 1{\cdot}00$, heading = 90·00°

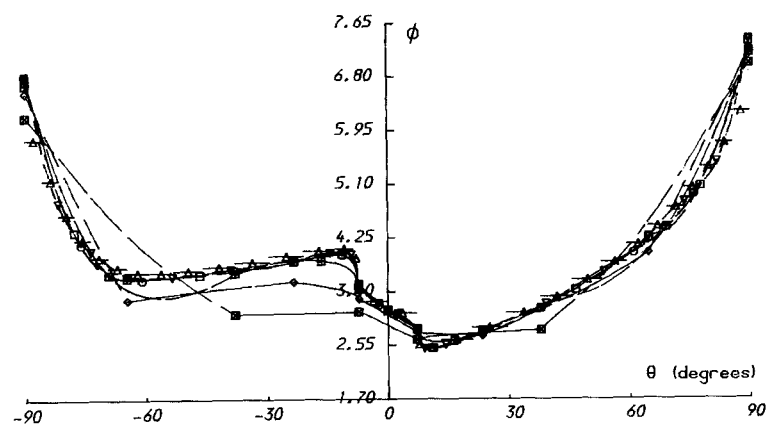

Figure 16(b). Out-of-phase diffraction velocity potential (section A); $\omega^2 B/2g = 1{\cdot}00$, heading = 90·00°

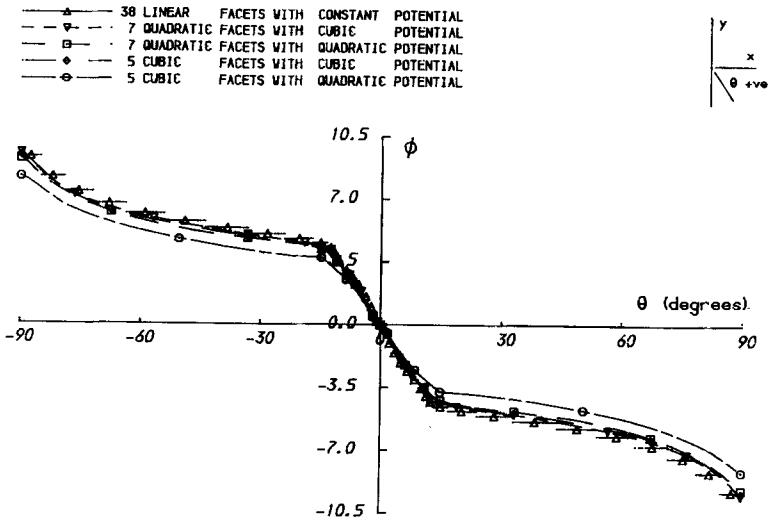

Figure 17(a). In-phase roll velocity potential (section B); $\omega^2 B/2g = 1{\cdot}00$

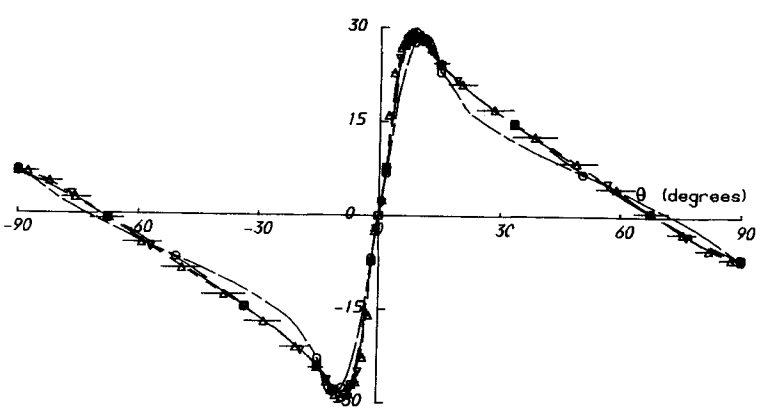

Figure 17(b). Out-of-phase roll velocity potential (section B); $\omega^2 B/2g = 1{\cdot}00$

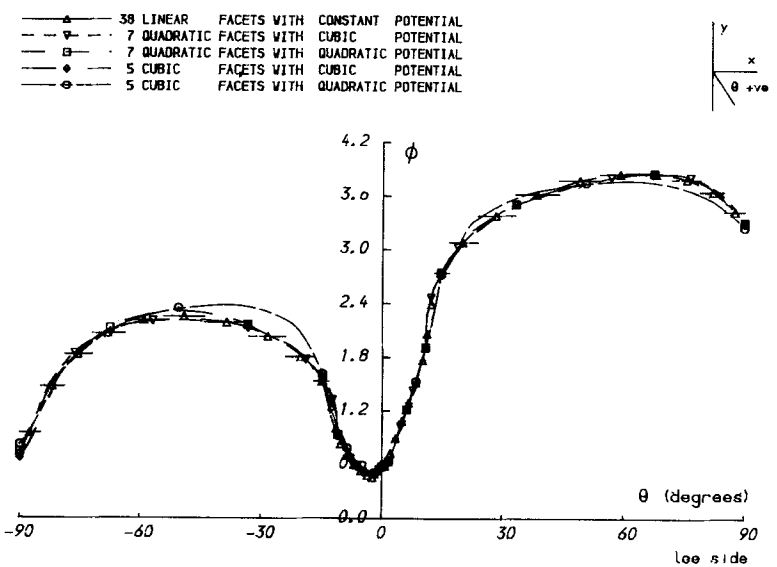

Figure 18(a). In-phase diffraction velocity potential (section B); $\omega^2 B/2g = 1{\cdot}00$, heading = 90·00°

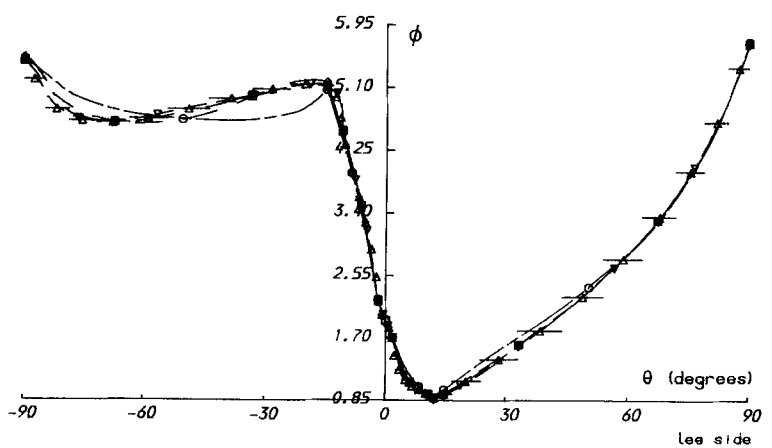

Figure 18(b). Out-of-phase diffraction velocity potential (section B); $\omega^2 B/2g = 1{\cdot}00$, heading = 90·00°

and 16 respectively for an $\omega^2 B/2g$ value of 1·0. As can be seen from the graphs, all HOBE models, except those with a linear approximation of the potential, follow very closely the results of the Frank close-fit method using a fine discretization. The same is also true for the sway and heave velocity potentials, which are not shown. For higher values of $\omega^2 B/2g$ the agreement tends to deteriorate somewhat, particularly with a linear approximation of the potential. This is almost certainly attributable to the influence of the irregular frequencies, as indicated by the sectional hydrodynamic coefficient results presented in Section 6.4.1. The results for section B, given in Figures 17 and 18, show the same trends observed in the results for section A.

6.4.3. CPU time comparisons. Comparisons of the CPU time required to set up and solve the linear simultaneous equations for the various discretizations used and for several $\omega^2 B/2g$ and wave period values are presented in Tables I–IV. The CPU times enclosed in parentheses represent the addition of the set-up and solution times. This is probably the more relevant quantity as it indicates whether any overall savings result from using HOBE formulations.

The time comparisons for sections A and B are presented in Tables I and II respectively. The first thing to be noted is how the set-up time more than doubles when using analytic integration instead of the mid-point rule in the standard Frank close-fit method. This clearly illustrates the point made in Section 5 regarding the assessment of time comparisons between the HOBE formulations and the standard method. Another point to be noted is that for the standard Frank close-fit method, with a practical number of facets, the set-up and solution time are of the same order of magnitude. Therefore, when using analytic integration, the set-up time will be approximately twice the solution time.

It is a well known fact that the set-up time varies as M^2 and the solution time as M^3, where M is

Table I. CPU times (milliseconds) section A

	Equations set-up time					
$\omega^2 B/2g =$	0·1	1·0	2·0	4·0	6·0	Solution time
Frank 22F standard	38 (92)	48 (102)	56 (110)	68 (122)	79 (133)	54
Frank 22F Analytic integration	105 (159)	125 (179)	141 (195)	166 (220)	191 (245)	54
7Q–CB	284 (338)	355 (409)	375 (429)	524 (578)	661 (715)	54
7Q–Q	174 (193)	209 (288)	233 (252)	286 (305)	396 (415)	19
7Q–L	77 (81)	110 (114)	125 (129)	149 (153)	183 (187)	4
5CB–CB	200 (222)	269 (291)	301 (323)	353 (375)	457 (479)	22
5CB–Q	126 (135)	157 (166)	180 (189)	234 (243)	264 (273)	9
5CB–L	62 (64)	76 (78)	80 (82)	120 (122)	136 (138)	2

Value in parentheses = set-up + solution time.

Table II. CPU times (milliseconds) section B

$\omega^2 B/2g =$	Equations set-up time 0·1	1·0	2·0	4·0	6·0	Solution time
Frank 20F Standard	32 (74)	43 (85)	52 (94)	66 (108)	77 (119)	42
Frank 20F Analytic integration	88 (130)	110 (152)	128 (170)	158 (200)	183 (225)	42
7Q–CB	318 (372)	415 (469)	517 (571)	699 (753)	828 (882)	54
7Q–Q	190 (209)	238 (257)	294 (313)	435 (454)	541 (560)	19
7Q–L	81 (85)	117 (121)	143 (147)	192 (196)	255 (259)	4
5CB–CB	220 (243)	298 (321)	358 (381)	503 (526)	584 (607)	23
5CB–Q	135 (144)	187 (196)	229 (238)	301 (310)	377 (386)	9
5CB–L	61 (63)	80 (82)	105 (107)	144 (146)	192 (194)	2

Value in parentheses = set-up + solution time.

the number of collocation points. Thus by reducing the total number of collocation points through using HOBE formulations, substantial time reductions in the solution of the equations will result. Because of the iterative nature of the integration procedure currently adopted in the HOBE program, the set-up time of the equations does not experience a similar reduction. This can be clearly seen in Tables I and II, where the set-up time for the HOBE formulations is substantially higher than that for the standard Frank close-fit method with analytic integration. An exception to this is the case of HOBE formulations with a linear approximation of the potential, where the times are comparable. It is also noticeable that the set-up time increases more rapidly with frequency for HOBE formulations than is the case for the Frank close-fit method.

Considering the total times, shown in parentheses, it can be seen that only the HOBE formulations with a linear approximation of the potential show competitive times. In some cases they even out perform the Frank close-fit method using the mid-point rule. Unfortunately, as indicated in Sections 6.4.1 and 6.4.2, these HOBE formulations also produce results of poor accuracy. All other HOBE formulations which produce practical results have total times which are in general greater than the total time for the Frank close-fit method using analytic integration.

The corresponding CPU time comparisons for the semi-submersible pontoon sections are shown in Tables III and IV for corner radii of 1·0 m and 4·0 m respectively. As can be seen, the same remarks made for sections A and B also apply in this case.

Finally, it should be noted that the calculations for the semi-submersible pontoon section were performed on an IBM 370/168 8 megabyte computer and those for sections A and B on an Amdahl 5860 40 megabyte computer. This explains the difference in the order of magnitude exhibited by the times in Tables I–IV.

Table III. CPU times (milliseconds) for semi-submersible pontoon section with corner radius = 1·0 m

Wave period	Equations set-up time 2	6	10	15	20	Solution time
Frank 56F Analytic inegration	4505 (7999)	6534 (10028)	4810 (8304)	4245 (7739)	3957 (7451)	3494
32Q–Q	21185 (26325)	26682 (31822)	18136 (23276)	14669 (19809)	14170 (19310)	5140
32Q–L	9989 (10694)	10666 (11371)	7141 (7846)	6238 (6943)	5614 (6319)	705

Values in parentheses = set-up + solution time.

Table IV. CPU times (milliseconds) for semi-submersible pontoon section with corner radius = 4·0 m

Wave period	Equations set-up time 2	6	10	15	20	Solution time
Frank 40F Analytic integration	2323 (3653)	3373 (4703)	2508 (3838)	2189 (3519)	2044 (3374)	1330
12Q–Q	5952 (6266)	4205 (4519)	3150 (3464)	2801 (3115)	2686 (3000)	314
12Q–L	3035 (3084)	2077 (2126)	1555 (1604)	1319 (1368)	1208 (1257)	49

value in parentheses = set-up + solution time.

7. CONCLUSIONS AND FINAL COMMENTS

The results presented are generally encouraging so far as the latent potential of the higher-order formulations is concerned. A fuller benefit would ideally require a significant reduction in the cost of the method as measured by CPU time. On the other hand, the number of collocation points used in 2D problems is generally so small that it is almost an impractical demand for the savings in solution time to exceed the increase in numerical calculation and program management costs when fully integrating the complex Green function and associated derivatives over the facets, including the full variation of the boundary conditions over the elements and permitting dial-up choice of order of function for geometry and velocity potential representation. However, some improvements could be made in the areas of numerical quadrature provided implementable and robust rules for automatic selection of domain subdivision and the correct order of quadrature approximation could be determined to provide evaluations of guaranteed maximum numerical error. From the point of view of the results produced, the method has shown that it is quite capable of producing the same accuracy with substantially less facets and/or collocation points. The applications undertaken suggest that the number of facets selected and their geometric description should be determined by the requirements of closely approximating the geometry of the section. The order of

approximation for the unknown velocity potential can be selected with a view to halving the number of collocation points used in the standard method. Obviously this choice is aimed at achieving a reduction in time for a given level of accuracy of the hydrodynamic coefficients. If the main concern of the analysis is the detailed fluid pressure over the section, then more facets with higher-order formulations should be used irrespective of the time expenditure.

One particular aspect which does require further expert treatment is the automatic selection of appropriate numerical integration. The present method of iterative Gaussian integration is somewhat wasteful in terms of integrand evaluation. As remarked earlier, some means of predicting the number of points to be used or where to start the iteration as a function of the source point, field point and facet attributes would considerably reduce the set-up time.

The mixing of facets with different orders of approximation for the geometry or the unknown velocity potential is something that could be tried to improve the flexibility of the method. However, the associated increase in the number of possible discretization parameters for a given section might create confusion for inexperienced users.

The HOBE method presented provides continuous solutions over the wetted surface of the structure. This can be advantageous when interfacing with structural analyses when discretizations suitable for hydrodynamic analyses provide hydrodynamic pressure loadings at points other than the nodes of the structural representation of the FE analysis, say. We can now avoid troublesome interpolation of the hydrodynamic pressures based on non-continuous solutions.

Some work on the 3D HOBE procedure has been undertaken and here the quadrature problems are compounded because of the need to evaluate surface integrals. However, the fact that the problems are one or two orders of magnitude greater in terms of the algebraic problems solved does mean that the solution time reduction will be significantly larger and therefore there is greater potential for overall time savings from the differentials of set-up and solution times.

ACKNOWLEDGEMENTS

We gratefully acknowledge the support of the SERC MTD under grant GR/B/8869.3 and the SERC MTD supported Dynamics of Compliant Structures Cohesive Programme, GR/C/7135.4. Miss Fiona Summers is thanked for her typing and editorial work under difficult circumstances.

APPENDIX. 2D SHAPE FUNCTIONS AND DERIVATIVES

Shape function definition	*Shape function derivatives*
Constant	
$N_1(t) = 1$	$N'_1(t) = 0$
$t_1 = 0$	
Linear	
$N_1(t) = \frac{1}{2}(1 - t)$	$N'_1(t) = -\frac{1}{2}$
$N_2(t) = \frac{1}{2}(1 + t)$	$N'_2(t) = +\frac{1}{2}$
$t_1 = -1, \quad t_2 = 1$	
Quadratic	
$N_1(t) = \frac{1}{2}t(t - 1)$	$N'_1(t) = t - \frac{1}{2}$

$N_2(t) = (1-t)(1+t)$ $\qquad N'_2(t) = -2t$

$N_3(t) = \frac{1}{2}t(t+1)$ $\qquad N'_3(t) = t + \frac{1}{2}$

$t_1 = -1, \quad t_2 = 0, \quad t_3 = 1$

Cubic

$N_1(t) = \frac{9}{16}(t-1)(t^2 - \frac{1}{9})$ $\qquad N'_1(t) = -\frac{9}{16}[t(3t-2) - \frac{1}{9}]$

$N_2(t) = -\frac{27}{16}(t - \frac{1}{3})(1-t^2)$ $\qquad N'_2(t) = -\frac{27}{16}[1 - t(3t - \frac{2}{3})]$

$N_3(t) = \frac{27}{16}(t + \frac{1}{3})(1-t^2)$ $\qquad N'_3(t) = \frac{27}{16}[1 - t(3t + \frac{2}{3})]$

$N_4(t) = \frac{9}{16}(t+1)(t^2 - \frac{1}{9})$ $\qquad N'_4(t) = \frac{9}{16}[t(3t-2) + \frac{1}{9}]$

$t_1 = -1, \quad t_2 = -\frac{1}{3}, \quad t_3 = \frac{1}{3}, \quad t_4 = 1$

REFERENCES

1. J. L. Hess and A. M. O. Smith, 'Calculation of non-lifting potential flow about arbitrary three-dimensional bodies', *Douglas Aircraft Company, Report ES40622*, 1962.
2. W. Frank, 'Oscillations of cylinders in or below the free surface of deep fluids', *NSRDC Report 2375*, 1967.
3. G. E. Hearn and K. C. Tong, 'Evaluation of Low Frequency Wave Damping', *Paper OTC 5176*, Houston, May 1986.
4. C. T. H. Baker, *The Numerical Treatment of Integral Equations*, Oxford University Press, 1977.
5. L. M. Delves and J. Walsh, *Numerical Solution of Integral Equations*, Oxford University Press, 1974.
6. M. B. Okan and S. M. Umpleby, 'The use of B-splines for the calculation of two-dimensional flow around arbitrary bodies', *Int. Shipbuilding Prog.*, **32**, 151–155 (1985).
7. M. B. Okan and S. M. Umpleby, 'Free surface flow around arbitrary two-dimensional bodies by B-splines', *Int. Shipbuilding Prog.*, **32**, 182–187 (1985).
8. J. L. Hess, 'Higher-order numerical solution of the integral equation for the two-dimensional Neumann problem', *Comput. Methods Appl. Mech. Eng.*, **2**, 1–15 (1973).
9. C. A. Brebbia, J. C. F. Telles and L. C. Wrobel, *Boundary Element Techniques: Theory and Application in Engineering*, Springer, New York 1984.
10. O. C. Zienkiewicz, *The Finite Element Method*, McGraw-Hill, New York, 1977.
11. M. G. Lean and A. Wexler, 'Accurate numerical integration of singular boundary element kernels over boundaries with curvature', *Int. j. numer. methods eng.*, **21**, 211–228 (1984).
12. A. H. Stroud and D. Secrest, *Gaussian Quadrature Formulas*, Prentice-Hall, Englewood Cliffs, NJ, 1966.
13. T. N. L. Patterson, 'The optimum addition of points to quadrature formulae', *Math. Comput.*, **22**, 847–856 (1968).